Octave and Decade Printed UWB Rectifiers Based on Nonuniform Transmission Lines for Energy Harvesting

John Kimionis, *Student Member, IEEE*, Ana Collado, *Senior Member, IEEE*, Manos M. Tentzeris, *Fellow, IEEE*, and Apostolos Georgiadis, *Senior Member, IEEE*

***Abstract*— Ambient RF energy harvesting is a potential energy source for low-power and battery-less wireless sensors, enabling a range of applications from monitoring to security as part of the Internet-of-Things (IoT) scenario. One of the main challenges of ambient RF energy harvesting is the requirement of operation over a multitude of frequency bands of low ambient power densities resulting in a very wide aggregate operating bandwidth. In this paper, design examples of novel ultra-wideband energy harvesters are demonstrated with octave and decade bandwidths in the UHF and low microwave spectrum. The RF-dc conversion efficiency is maximized by tailoring the dimensions of a nonuniform transmission line used to provide broadband impedance matching. The design challenges in terms of impedance matching based on the Bode–Fano theoretical limit, losses and miniaturization are highlighted. Two prototypes are presented and their performance is evaluated. The octave band rectifier showed a measured RF-dc conversion efficiency of more than 60% over a frequency band of 470 to 860 MHz at 10-dBm input power. The decade band rectifier fabricated on Kapton substrate using inkjet printing featured a higher than 33% efficiency over a frequency band from 250 MHz to 3 GHz at 10-dBm input power.**

***Index Terms*— Flexible electronics, inkjet printing, Internet of Things (IoT), nonuniform transmission line, rectifier, RF energy harvesting, ultra-wideband (UWB), wireless power transfer.**

I. Introduction

HARVESTING ambient RF energy to power wireless sensors and transmitters has been receiving significant attention, due to an increasing interest in compact, low power, and even battery-less sensors. Such Internet-of-Things (IoT) devices will serve a growing number of applications from smart metering and monitoring in general to security, health, and well-being [1]. There is a significant amount of publications in the recent literature regarding the performance analysis of rectennas and rectifiers, especially due to the recent interest in energy harvesting and wireless powering for IoT applications [1], [2]. There are several important earlier works on diode detectors [3], and theoretical estimation of the efficiency of diode rectifiers [4], as well as more recent publications such as [5]–[7] addressing the performance as RF-dc power conversion circuits in low-power far-field wireless power transfer or RFID applications.

There are several examples in the recent literature demonstrating the ability to power sensors using the energy available from various broadcast transmitters including, FM, TV, cellular, or Wi-Fi systems [8], [9]. One characteristic of such transmissions is the time-/space-varying variable nature of the available power density, due to a variety of reasons such as complex propagation settings as well as varying demand and broadcasting schedules. As a result, one has to be able to harvest RF energy within a large aggregate spectrum to guarantee the harvesting of sufficiently high aggregate power for practical applications. In rectenna and rectifier design, it is a challenge to maximize the RF-dc conversion efficiency over a wide aggregate bandwidth including multiple narrower frequency bands or an ultrawide single frequency band. This is important in order to maximize the total harvested RF energy from broadcast transmissions at different frequencies. Recent publications of dual band, triple, or quadruple band rectifier circuits include [10]–[12] and 3-D topologies have been recently explored for harvesting RF power from multiple directions [13] without compromising communication [14].

In order to address the wideband harvesting requirement, a novel ultra-wideband (UWB) rectifier is introduced in this paper. The equivalent *RC* circuit of different rectifiers for a variety of different input power excitation and output load values is extracted and the theoretical minimum reflection coefficient over a desired frequency band based on the Bode–Fano theory [15] is investigated. Based on this study a rectifier circuit topology is selected and its impedance matching circuit is designed in a broadband way. A nonuniform microstrip transmission line in series with an inductor is selected to implement the matching network and harmonic balance optimization is used to maximize the RF-dc rectifier efficiency. Preliminary results of this paper are presented in [16], where a rectifier circuit with an octave bandwidth was designed. In this paper, in addition to further design and optimization details of the aforementioned rectifier, a second rectifier design is presented covering more than a decade bandwidth. Additionally, the proposed rectifier is simultaneously

Manuscript received February 23, 2017; accepted April 9, 2017. Date of publication May 11, 2017; date of current version November 3, 2017. The work of J. Kimionis and M. M. Tentzeris was supported in part by the National Science Foundation and in part by the Defense Threat Reduction Agency. The work of A. Collado and A. Georgiadis was supported in part by EU H2020 Marie Sklodowska-Curie under Grant 661621 and in part by COST Action IC1301 Wireless Power Transmission for Sustainable Electronics.
(Corresponding author: John Kimionis.)

J. Kimionis and M. M. Tentzeris are with the School of Electrical and Computer Engineering, Georgia Institute of Technology, Atlanta, GA 30332 USA (e-mail: ikimionis@gatech.edu; etentze@ece.gatech.edu).

A. Collado and A. Georgiadis are with the School of Engineering and Physical Sciences, Heriot-Watt University, Edinburgh EH14 4AS, U.K. (e-mail: apostolos.georgiadis@ieee.org; ana.collado@ieee.org).

Color versions of one or more of the figures in this paper are available online at http://ieeexplore.ieee.org.

Digital Object Identifier 10.1109/TMTT.2017.2697851

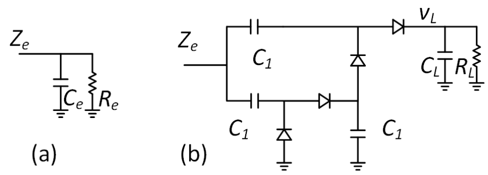

Fig. 1. Rectifier input impedance. (a) Equivalent circuit. (b) Charge-pump rectifier with four diodes.

optimized in order to minimize its size and a flexible substrate and inkjet printing fabrication are used to demonstrate a proof-of-concept conformal implementation using low-cost additive manufacturing. Prototypes of the two rectifiers have been fabricated and tested showing good agreement with simulations. The octave band rectifier has an RF-dc conversion efficiency varying within [5.5%, 13.5%] from 475 to 975 MHz for −20-dBm input available power, and more than 60% efficiency from 470 to 860 MHz when the input power is 10 dBm. The decade rectifier has an efficiency within [4.5%, 7%] for −10-dBm input power and more than 33% for 10 dBm input power between 250 MHz and 3 GHz, for a load of 1.3 kΩ.

The paper is structured as follows: in Section II, the equivalent circuit of different generic rectifier architectures is derived and the minimum reflection coefficient is evaluated based on the Bode–Fano theory. In Section III, the design and optimization procedure of the nonuniform transmission line matching network are described and two rectifiers with an octave and decade bandwidth, respectively are presented. Finally, Section IV presents a summary of this work's results.

II. Bode–Fano Reflection Coefficient Limit for UWB Rectifier Impedance Matching

According to the theory originally developed by Bode and extended by Fano [15], the minimum reflection coefficient magnitude $|\Gamma_m|$ which can be obtained by a lossless matching network connected to a load impedance consisting of a shunt resistor R_e and a shunt capacitor C_e over a bandwidth B is limited by

$$|\Gamma_m| \geq e^{-\frac{1}{2BR_eC_e}} \tag{1}$$

where a constant reflection coefficient $|\Gamma_m|$ over the bandwidth B and unity reflection coefficient over the rest of the spectrum is assumed.

The input impedance of a series diode rectifier or charge-pump (voltage N-tupler) rectifier, such as the ones shown in Fig. 1, for a given input power and output load resistance is equivalent to the input impedance of a shunt RC circuit. This can be easily verified using a commercial nonlinear circuit simulator such as harmonic balance.

In a first example [16], the equivalent circuits of different rectifier circuits of a series diode topology and of different charge pump rectifiers with two, four, and six diodes were evaluated. The rectifier circuit capacitors $C_1 = 100$ pF and $C_L = 10$ nF were set to sufficiently large values to represent an effective short circuit at the frequency band 0.4–1 GHz under consideration. It was shown that the equivalent capacitance C_e was proportional to the number of diodes and approximately independent of the output load resistance and of the input power values [16]. The equivalent diode resistance R_e was approximately inversely proportional to the number of diodes and depended both on the input power level and the output load resistance [16]. Due to this fact, the product of R_e and C_e depends on the number of diodes in the rectifier circuit and consequently the minimum reflection coefficient (1) depends on the input power, the output load resistance as well as on the number of diodes.

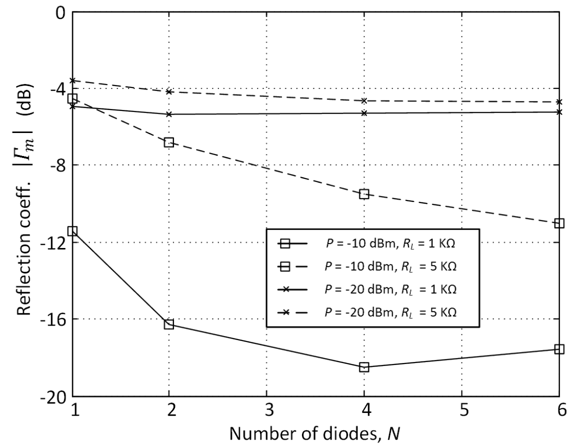

Fig. 2. Theoretical minimum reflection coefficient in the frequency band of 0.4–1.0 GHz versus the number of diodes for different input power and output load resistance values.

The minimum reflection coefficient obtained using (1) for frequency band of 0.4–1 GHz is plotted in Fig. 2. One can see that it is easier to minimize the reflection coefficient at higher input power levels and at lower load resistance values. Furthermore, the series diode rectifier appears to be more difficult to match than rectifier charge-pump circuits with more diodes. Based on the result of Fig. 2, a rectifier with four diodes was selected in order to design an energy harvester covering the band from 0.4 to 1 GHz.

The equivalent input resistance and capacitance of various rectifier circuits with $N = 1, 2, 4,$ and 6 diodes and load resistance $R_L = 1$ kΩ are plotted versus the available input RF power P in Fig. 3. One can see that the nonlinear nature of the capacitance becomes evident for power levels near 0 dBm and above. In addition, the strong dependence of the input resistance on the input power is evident.

In a second more broadband example, a rectifier with a more-than-decade bandwidth from approximately 0.25 to 3 GHz was considered. Using the obtained equivalent resistance and capacitance values and (1), contours of theoretical minimum reflection coefficient were computed for different load resistance input power and number of rectifier diodes, as shown in Fig. 4. Once again it is verified that a lower reflection coefficient can be theoretically obtained for higher input power levels and smaller load values. Furthermore, the series diode rectifier is more difficult to match, while there is little improvement going from four- to six-diode rectifiers. In order to maintain a minimum circuit complexity a two-diode rectifier was selected for the decade band design.

III. Ultra-Broadband Rectifier Design

A nonuniform transmission line in series with a lumped inductor L_1 was chosen to implement the impedance matching

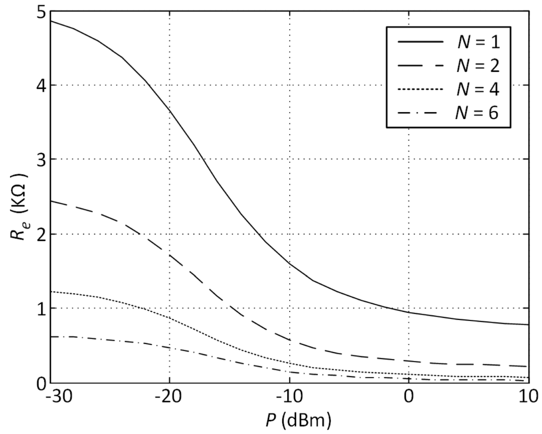

(a)

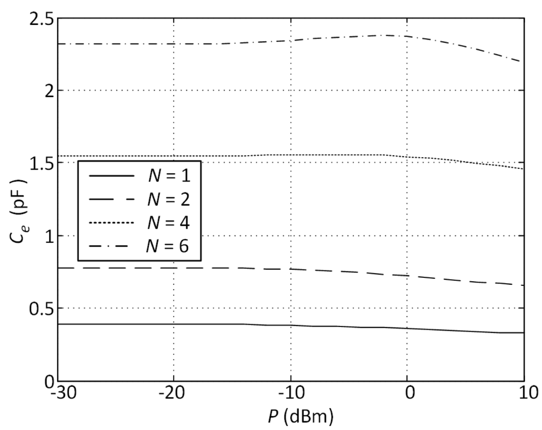

(b)

Fig. 3. Rectifier equivalent input impedance versus input power. (a) Resistance and (b) capacitance for rectifiers with a different number of diodes N. The output load resistance is 1 kΩ.

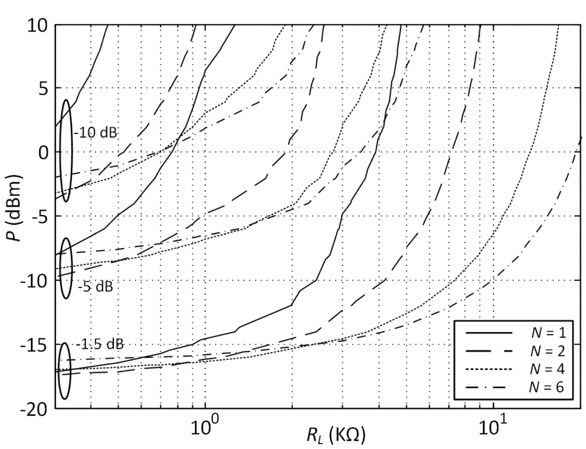

Fig. 4. Rectifier minimum reflection coefficient (dB) contours versus input power and load resistance for UWB rectifier circuits with a different number of diodes N.

network for the introduced ultrabroadband rectifier. Nonuniform transmission lines have been traditionally used to provide broadband matching to real loads as shown by the selected examples of [17] and [18]. In addition, they can be used to provide dispersion compensation in optical communication links [19]. In this paper, a series inductor is first used to provide narrowband matching and cancel the capacitive imaginary part of the rectifier impedance around a certain frequency within the band under consideration. Then a nonuniform transmission line transforms the low-imaginary-part complex impedance to the desired 50-Ω source impedance. The matching network is shown in Fig. 5. A microstrip line consisting of trapezoidal sections was used to implement the nonuniform transmission line. Coplanar waveguide or grounded coplanar waveguide lines can also be used, however, microstrip line was chosen for the proof-of-concept prototypes in order to minimize fabrication time and minimize the need for plated through via holes or bridges.

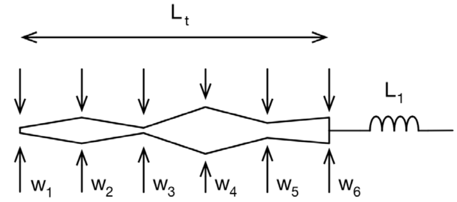

Fig. 5. Rectifier impedance matching network consisting of a series inductor and a nonuniform transmission line.

The rectifier RF-dc conversion efficiency is defined as

$$\eta = \frac{P_{\mathrm{dc}}}{P} \tag{2}$$

where $P_{\mathrm{dc}} = V_L^2/R_L$ and V_L are the output dc voltage and R_L the output load resistance. P is the available RF power at the input of the rectifier. In this effort, η is maximized over the broadest desired frequency band for a given input power P using harmonic balance optimization while optimization parameters include the nonuniform transmission line, the inductor L_1 and the load R_L.

A. Octave Bandwidth Rectifier

As a proof-of-concept, an octave bandwidth rectifier for the 400-MHz–1-GHz band was designed using a four diode charge-pump rectifier and a nonuniform transmission line of length L_t consisting of five trapezoidal sections of equal length as shown in Fig. 5. The Skyworks SMS7630 diode was used, and the package parasitics were taken into account for the design process. A parasitic inductance value of $L_p = 0.6$ nH and a parasitic capacitance value of $C_p = 0.25$ pF provided by the manufacturer were added in the design schematic [Fig. 6 (top)]. The selected substrate was Arlon A25N with dielectric permittivity 3.38, loss tangent 0.0025, and 20-mil thickness. The minimum linewidth in the optimization process was set to 0.3 mm in order to facilitate fabrication with a circuit mill. The full rectifier schematic is shown in Fig. 6 (middle), with the matching network including the five-section nonuniform transmission line and the series lumped inductor L_1. Coilcraft inductors were used for the designs, with all surface mount device (SMD) package parasitics accounted in the simulations and optimization. The circuit parameters were optimized with keysight advanced system (ADS) in harmonic balance mode using gradient optimization, with a goal of maximizing the efficiency value η.

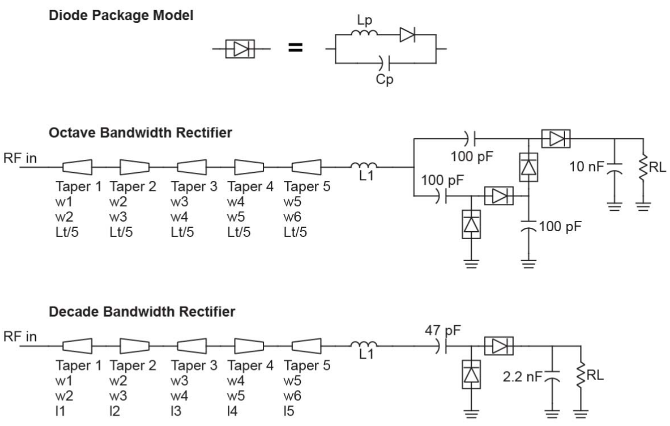

Fig. 6. Top: SMS730 diode parasitic model. Middle: optimization schematic for octave bandwidth rectifier with nonuniform transmission line. Bottom: optimization schematic for decade bandwidth rectifier with nonuniform transmission line.

TABLE I
RECTIFIER OPTIMIZATION PARAMETERS $P = -20$ dBm

Param.	Value	Param.	Value
w_1	2.65 mm	w_6	6 mm
w_2	2.72 mm	L_t	174.5 mm
w_3	3.62 mm	L_1	20 nH
w_4	6 mm	R_L	12.2 kΩ
w_5	1 mm		

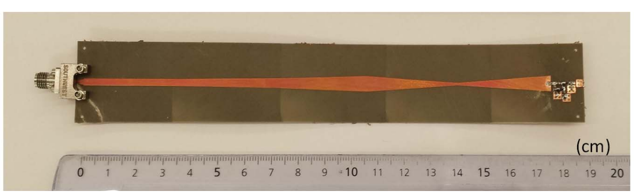

Fig. 7. Octave bandwidth rectifier prototype.

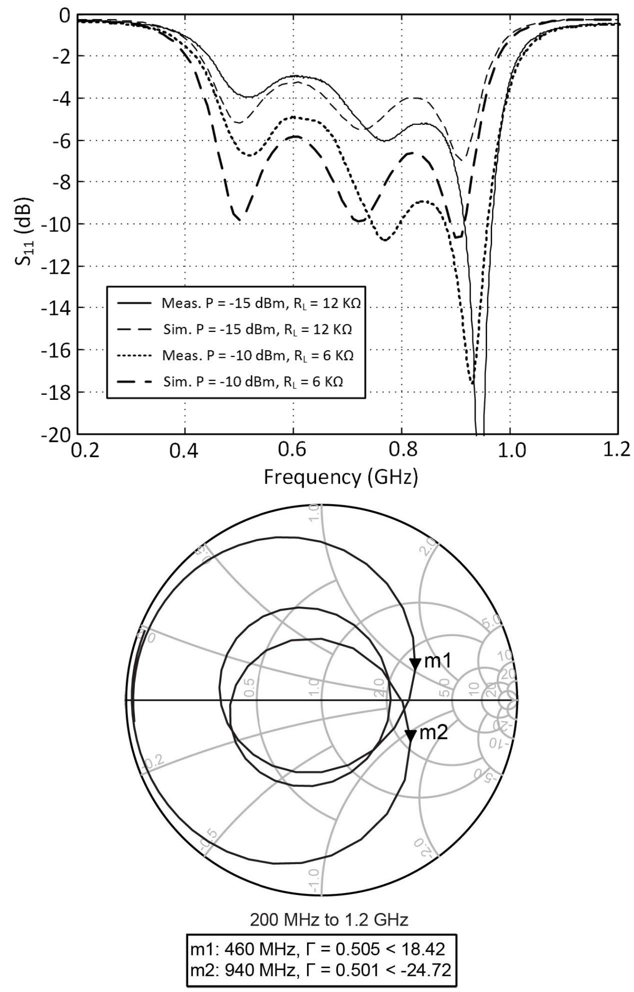

Fig. 8. Input S-parameters of the octave band rectifier. Top: return loss. Bottom: S_{11} Smith chart for input power $P = -10$ dBm and $R_L = 7$ kΩ.

Note that this does not necessarily optimize the return loss S_{11}, since the main goal of the rectifier is to deliver as much power to the load R_L as possible, rather than minimize reflections at the RF input port. The initial value of the total line length L_t was arbitrarily set to 15 cm and was allowed to optimize. This value corresponds to an electrical length of approximately 185° at 632 MHz which is the geometric mean between the operating band edges of 0.4 and 1 GHz. For this octave bandwidth rectifier, all transmission line sections were equal, with length $L_t/5$.

Table I shows the result of the optimization process including the final dimensions of the transmission line sections, the inductor value, and the optimum load at -20 dBm input power. The fabricated prototype, shown in Fig. 7, was measured with a lab setup to characterize the input S-parameters and conversion efficiency for different power levels and load values. The input S-parameter measurements were obtained using a network analyzer in frequency sweep mode and varying port power. The RF-dc conversion efficiency measurements were obtained using a signal generator to provide a continuous wave signal at a given power level and the dc output voltage was measured using a digital multimeter (DMM). The output load was set using a trimmer resistor and measured using the DMM. The RF power level at the input of the rectifier was measured using a spectrum analyzer and cable losses were characterized using a network analyzer/cable tester. The dc output voltage value was converted to output power value using the measured load resistance and the efficiency was calculated as the ratio of (2).

The rectifier's input S-parameters are shown in Fig. 8 (top), where a good agreement between simulation and measurements is obtained. In accordance with Section II, one can see that as the input power increases and the rectifier output load resistance decreases, impedance matching is improved. For power levels of 0 and 10 dBm and respective load values of 5.5 and 3 kΩ, the return loss is better than -10 dB within the whole band of interest, and the curves have been omitted for clarity. As aforementioned, the optimization goal for the rectifier was the maximum efficiency and not minimized return loss. Thus, the curves of Fig. 8 (top) can be used for relative comparison of the rectifier's behavior under different input power levels and output load values. Fig. 8 (bottom) shows the input reflection coefficient in Smith chart form for an input power level of -10 dBm and a load value of $R_L = 7$ kΩ.

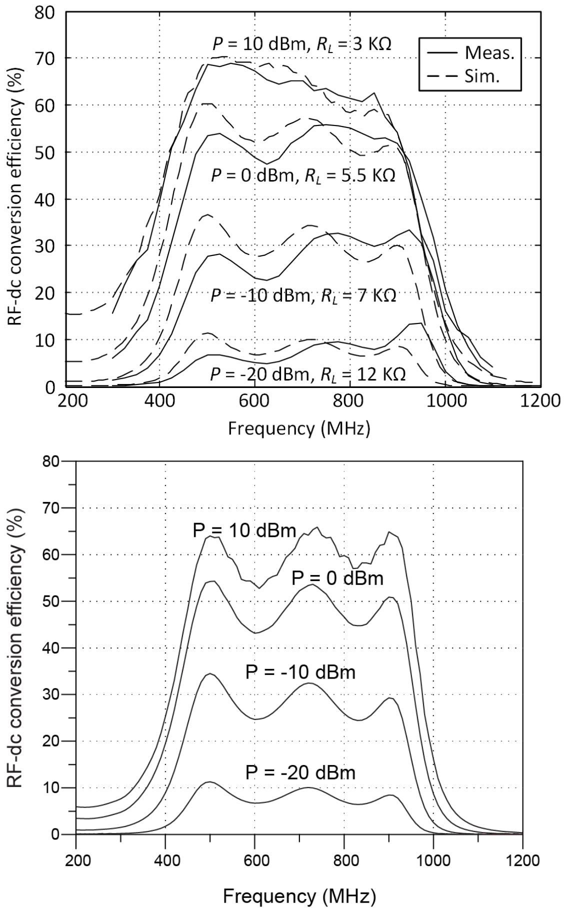

Fig. 9. Octave bandwidth rectifier RF-dc conversion efficiency. Top: measurement and simulation for varying power levels and optimal load per power level. Bottom: simulation for varying power levels and fixed load value of 12 kΩ.

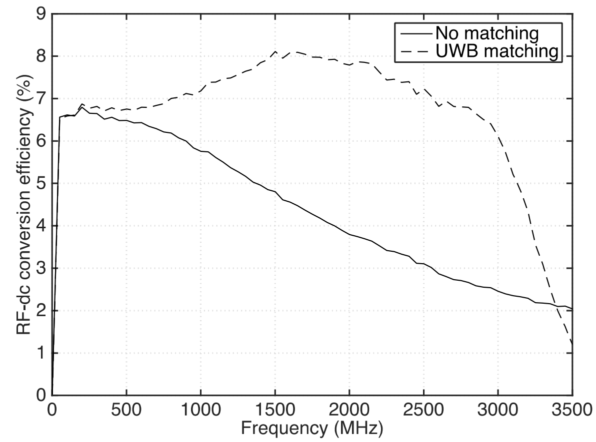

Fig. 10. Rectifier RF-dc conversion efficiency without and with UWB matching (RF input power −10 dBm, load value 1.3 kΩ).

The rectifier RF-dc conversion efficiency was evaluated for different input power levels and it is presented in Fig. 9 (top). The optimum load was also investigated experimentally and the plots of Fig. 9 (top) include the prototypes' load values chosen as close as possible to the optimum value based on the available resistors for the measurements. Simulation results are compared for the same load value at each given input power level showing a very good agreement. The measured efficiency varies from approximately 5.5% at 475 MHz to 13.5% at 975 MHz for an input power level of −20 dBm, exceeding an octave bandwidth of operation. In addition, the efficiency remains above 60% at 10 dBm input power over a bandwidth of 390 MHz, from 470 to 860 MHz. It is noted that the optimum load leading to maximum efficiency is reduced with increasing input RF power. This has been studied in detail in [20] and is consistent within the simulation and measurement results of this paper. In Fig. 9 (bottom), the simulated RF-dc conversion efficiency is also shown for varying input power levels from −20 to 10 dBm, for a fixed load value of $R_L = 12$ kΩ, which corresponds to the optimal load value for $P = -20$ dBm.

B. Decade Bandwidth Rectifier on Flexible Substrate

The decade bandwidth rectifier was designed to achieve its optimal operation at 3 GHz with an inkjet printing implementation on a flexible polyimide (Kapton) substrate with dielectric constant $\varepsilon_r = 3.4$, loss tangent $\tan\delta = 0.0025$, and 5-mil thickness. A two-diode rectifier is designed to drive a load of 1.3 kΩ with an input power level of as low as −10 dBm. The same diode was used (Skyworks SMS7630) for the decade bandwidth rectifier and ADS was used in harmonic balance mode to optimize the circuit of Fig. 6 (bottom) with a gradient optimization algorithm. The optimization goal is the maximization of the RF-dc conversion efficiency between 250 MHz and 3 GHz, without any target goal for the return loss.

A nonuniform transmission line is designed and optimized for the UWB rectifier for decade-broadband matching. The transmission line length is kept significantly low compared to the octave rectifier to minimize the losses of inkjet-printed traces that feature lower conductivity levels (5×10^6 S/m) compared to the copper cladding of standard PCBs (5.8×10^7 S/m). The microstrip line mainly targets the higher frequencies of the band, where diodes typically show low-efficiency performance. The effect of matching with the nonuniform transmission line can be clearly seen in Fig. 10, where the simulated RF-dc conversion efficiency of the two-diode rectifier driving a 1.3-kΩ load with and without UWB matching is shown for −10-dBm input power. "No matching" refers to the case of directly feeding the RF power to the voltage doubler without the lumped inductor and nonuniform transmission line. It is apparent that with the UWB matching network, consisting of the inductor L_1 and nonuniform transmission line, the average efficiency across the band is increased, with a peak around 1500 MHz that is the center of the band. Notice that the peak has a value of 8%, while an average efficiency of 7% spans a very wide frequency region of 3 GHz. This is in contrast with conventional harvesters that are optimized for a specific power and frequency point and achieve higher efficiency values, albeit around a very tuned frequency point. This has a result of a very sharp efficiency decay when the excitation signal is slightly detuned from the precisely-tuned operating point of the harvester. This work's decade bandwidth harvester features a steady efficiency value across a very wideband, which can facilitate the design of additional dc–dc converters,

TABLE II
UWB RECTIFIER OPTIMIZATION PARAMETERS, $P = -10$ dBm

Param.	Value	Param.	Value
w_1	1.76 mm	l_2	5.95 mm
w_2	0.24 mm	l_3	4.79 mm
w_3	0.11 mm	l_4	2.12 mm
w_4	0.23 mm	l_5	0.1 mm
w_5	3.43 mm	L_t	14.22 mm
w_6	1 mm	L_1	3.6 nH
l_1	1.25 mm	R_L	1.3 k

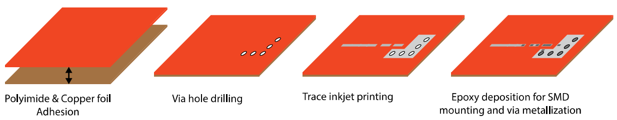

Fig. 11. Printed board fabrication process.

supercapacitor charging circuits, and power management units at the output of the harvester.

Due to the nature of inkjet printing, where high resolution of printed features can be achieved, the nonuniform transmission line for the UWB harvester was not constrained to a minimum width of 0.3 mm, as in the case of the octave band harvester fabricated on a rigid substrate. As shown in Table II, the smallest required width of the UWB matching line is 100 μm, which can be precisely achieved with inkjet printing. Moreover, for the UWB transmission line, the tapered sections do not all feature the same length, in order to double the degrees of freedom for the design and minimize any potential losses. The line sections' width (w_i) and length (l_i) values as well as the matching inductor value can be seen in Table II. The total line length is less than 1.5 cm, keeping the total system (harvester circuit and line) area less than 2 cm^2.

The fabrication of the decade UWB harvester prototype board, before placing the SMD components (0603 size), involves four steps, shown in Fig. 11 as follows.

1) Substrate preparation by attaching an adhesive copper foil (copper tape) under the polyimide film to form the microstrip ground plane.
2) Drilling to form the holes of the vias required for ground connections.
3) Inkjet printing of traces with a conductive silver nanoparticle (SNP) ink.
4) Conductive epoxy deposition for via metallization and SMD component attachment.

The holes on the substrate are drilled right after attaching the copper tape to the polyimide film and before printing the silver to avoid any cracks on the printed traces [Fig. 12 (left)]. Apart from the 0.8-mm-diameter holes drilled for vias, two 2-mm diameter holes are also drilled to mount an SMA end-launch connector.

A Dimatix DMP-2800 inkjet printer is used to deposit droplets of SNP ink on the substrate to form the traces of the nonuniform line and the circuit component pads. Five layers of SNP ink are deposited with 20-μm drop spacing on a 60 °C-hot platen and an interlayer printing delay of at

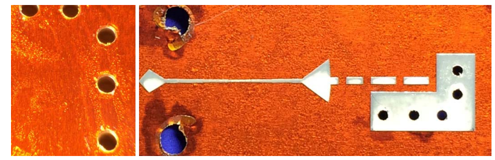

Fig. 12. Left: drilled via holes on polyimide and copper tape substrate. Right: inkjet-printed board; feeding section, nonuniform transmission line, and SMD components pads.

least 300 s, to guarantee enough time for SNP ink solvent evaporation which will minimize ink spreading. This is crucial, especially for the thinnest parts of the line, where the linewidth (100 μm) consists of only 4–5 SNP drops. The board is placed in a temperature-controlled oven at 180 °C for at least 60 min to ensure full SNP sintering that will maximize conductivity. The fully cured board can be seen in Fig. 12 (right), with the SNP ink printed directly on top of the vias.

It is interesting to note that printing directly on the drilled substrate creates SNP walls in the holes that electrically connect the printed silver traces with the copper ground plane. The resistance between the top silver trace and the copper ground plane is less than 4 Ω. However, a low resistivity silver epoxy (0.0007 $\Omega \cdot$cm) is used for via metallization to improve operation at high frequencies as well as for SMD component mounting. The epoxy consists of two parts that need to be mixed together to start the curing process. Due to the small SMD sizes (order of millimeters) a controlled dispensing method is needed to precisely deposit the conductive adhesive on the silver traces. A novel method is tested, inspired by solder paste deposition tools, that involves a solder paste deposition pump that applies air pressure to a syringe with a piston for microdispensing of paste on circuit traces. Because conductive epoxies are typically two-part materials that start curing immediately after mixing (even at room temperatures), the epoxy chosen has a long working time (4 h), which is enough for mixing, transferring to a 10-cc syringe tube, and connecting to the deposition pump for dispensing, before starting hardening up to a nonworking viscosity level. The pump pressure is set to at least 0.2 MPa to dispense the mixed epoxy with a 26-gauge tip. The via holes are filled with epoxy which accumulates on the via walls, creating shorts between the top printed traces and the copper ground plane. Drops of epoxy are also dispensed on the printed traces at the positions where the SMD pads are going to be attached. After placing the components, the board is oven heated at a moderate temperature of 65 °C for at least 60 min. A microscope photograph of the attached SMD components and metallized vias is shown in Fig. 13. The fully assembled harvester board (2.5 × 0.75 cm) with the attached end-launch connector is shown in Fig. 14.

The simulated input S-parameters along with the VNA-measured S-parameters of the UWB harvester prototype are shown in Fig. 15 (top) and a Smith chart of the input reflection coefficient is shown in Fig. 15 (bottom) for an input power of 0 dBm. A signal generator and a DMM have been used to measure the harvester output voltage level for various input power levels and frequency points. The 2-D function $V_{\text{out}} = f(F, P)$ contours are shown in Fig. 16 for

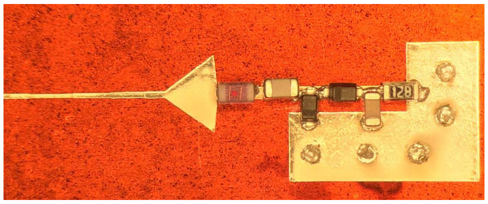

Fig. 13. Microphotograph of assembled harvester, with SMD components and epoxy-metallized vias.

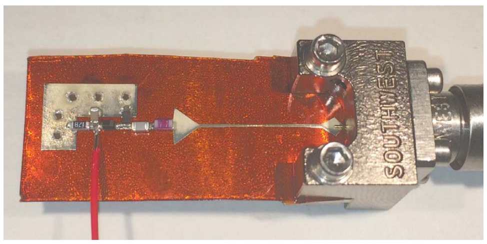

Fig. 14. Flexible UWB harvester prototype with end-launch SMA connector and V_{out} testing output.

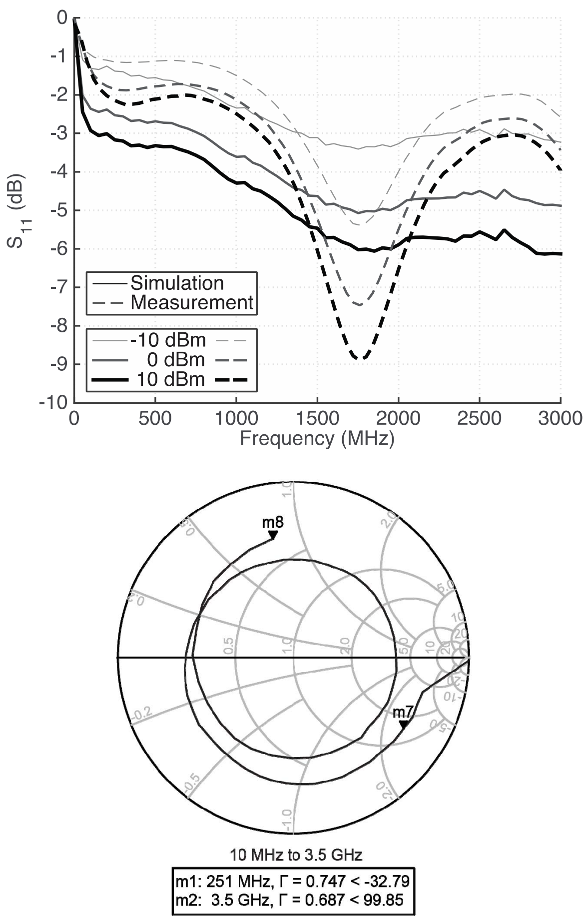

Fig. 15. Input S-parameters of the decade band rectifier (R_L = 1.3 kΩ). Top: return loss. Bottom: S_{11} Smith chart for input power $P = 0$ dBm and R_L = 1.3 kΩ.

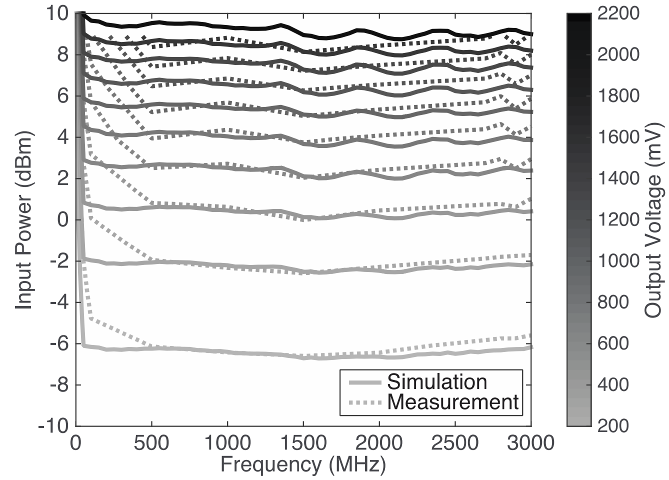

Fig. 16. Contours of simulated and measured rectifier dc output voltage for varying input power level and frequency values (R_L = 1.3 kΩ).

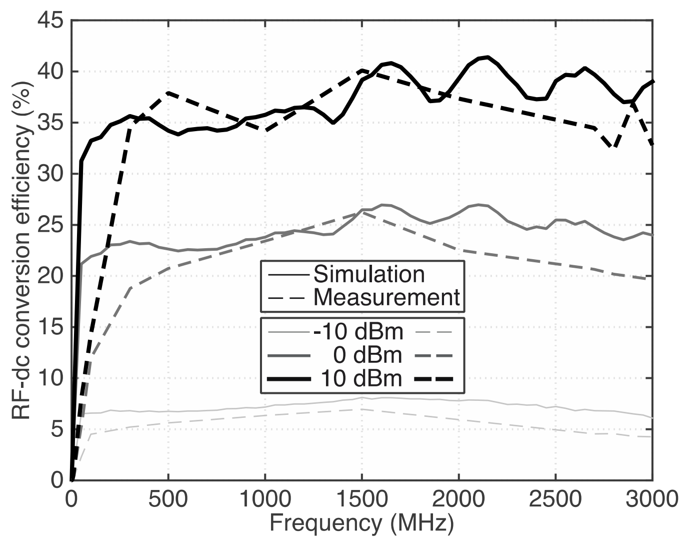

Fig. 17. Simulated and measured efficiency for UWB harvester (R_L = 1.3 kΩ).

the simulated circuit and measured prototype. The x-axis is the frequency variation and the y-axis is the input power variation. The tone of gray denotes the level (output voltage) of each contour, according to the color bar on the right, i.e., the output voltage increases as the input power increases for a given frequency, and the output voltage remains stable across frequency variations for any given input power level. It can be seen that the output power level for a given input power shows very little variation in the whole band of interest between 250 MHz to 3 GHz. In Fig. 17, the efficiency across the frequency band is plotted for three input power levels, −10, 0, and 10 dBm. The measured efficiency increases from 6% on average for −10-dBm input power to 37% on average for 10-dBm input power. The efficiency shows small variations within the band between 250 MHz and 3 GHz, between [4.5%, 7%] for an input power level of −10-dBm, [18%, 25%] for 0 dBm, and [32.5%, 40%] for 10-dBm input power. Even though the efficiency is increased for high power levels, there are applications where high-level RF power is available e.g., from handheld devices such as radios. The work in [21] has successfully demonstrated the exploitation of ambient nearby sources for powering up wearable devices.

In our work, we leverage the potential of such high power availability, by enabling an UWB operation of flexible printed harvesters that can be integrated with wearables and exploit power from handheld radios, cellphones, desktop Wi-Fi access points, etc. The harvested power can be used to support low-power sensor front-ends, such as backscatter modulators for sophisticated communication schemes [22].

In comparison with existing UWB rectifiers in the literature, both the octave and decade bandwidth rectifiers presented in this paper achieve RF-dc conversion efficiency values that are significantly flatter (less than 10% efficiency fluctuation) versus frequency variations for any given power level. As an example, the octave bandwidth rectifier presented in [23] achieves an RF-dc conversion efficiency that greatly varies from 20% to 80% for frequencies between 650 MHz and 1.05 GHz at a high input power level of +20 dBm and only achieves a flat efficiency value for varying frequency at its highest operating input power of 40 dBm.

IV. Conclusion

This paper has presented the design of UWB rectifiers that utilize nonuniform transmission lines for broadband matching. Two prototype harvesters have been implemented and characterized to prove the feasibility of UWB matching with nonuniform transmission lines. The first, which features a 4-diode charge pump and is implemented on a rigid substrate, achieved a measure RF-dc conversion efficiency of more than 60% for an octave frequency band of 470 to 860 MHz at 10-dBm input power. The second, which features a 2-diode charge pump and is inkjet printed on a flexible substrate targeting conformal applications, achieved an efficiency of more than 33% for an ultrawide frequency band between 250 MHz and 3 GHz.

References

[1] S. Kim *et al.*, "Ambient RF energy-harvesting technologies for self-sustainable standalone wireless sensor platforms," *Proc. IEEE*, vol. 102, no. 11, pp. 1649–1666, Nov. 2014.

[2] J. A. Hagerty, F. B. Helmbrecht, W. H. McCalpin, R. Zane, and Z. B. Popovic, "Recycling ambient microwave energy with broad-band rectenna arrays," *IEEE Trans. Microw. Theory Techn.*, vol. 52, no. 3, pp. 1014–1024, Mar. 2004.

[3] R. G. Harrison, "Full nonlinear analysis of detector circuits using Ritz–Galerkin theory," in *IEEE MTT-S Int. Microw. Symp. Dig.*, Albuquerque, NM, USA, Jun. 1992, pp. 267–270.

[4] T.-W. Yoo and K. Chang, "Theoretical and experimental development of 10 and 35 GHz rectennas," *IEEE Trans. Microw. Theory Techn.*, vol. 40, no. 6, pp. 1259–1266, Jun. 1992.

[5] J. A. G. Akkermans, M. C. V. Beurden, G. J. N. Doodeman, and H. J. Visser, "Analytical models for low-power rectenna design," *IEEE Antennas Wireless Propag. Lett.*, vol. 4, pp. 187–190, 2005.

[6] G. De Vita and G. Iannaccone, "Design criteria for the RF section of UHF and microwave passive RFID transponders," *IEEE Trans. Microw. Theory Techn.*, vol. 53, no. 9, pp. 2978–2990, Sep. 2005.

[7] S. D. Assimonis, S.-N. Daskalakis, and A. Bletsas, "Sensitive and efficient RF harvesting supply for batteryless backscatter sensor networks," *IEEE Trans. Microw. Theory Techn.*, vol. 64, no. 4, pp. 1327–1338, Apr. 2016.

[8] R. J. Vyas, B. B. Cook, Y. Kawahara, and M. M. Tentzeris, "E-WEHP: A batteryless embedded sensor-platform wirelessly powered from ambient digital-TV signals," *IEEE Trans. Microw. Theory Techn.*, vol. 61, no. 6, pp. 2491–2505, Jun. 2013.

[9] A. N. Parks, A. P. Sample, Y. Zhao, and J. R. Smith, "A wireless sensing platform utilizing ambient RF energy," in *Proc. IEEE Topical Conf. Biomed. Wireless Technol., Netw., Sens. Syst. (BioWireleSS)*, Jan. 2013, pp. 154–156.

[10] A. Collado and A. Georgiadis, "Conformal hybrid solar and electromagnetic (EM) energy harvesting rectenna," *IEEE Trans. Circuits Syst. I, Reg. Papers*, vol. 60, no. 8, pp. 2225–2234, Aug. 2013.

[11] B. L. Pham and A.-V. Pham, "Triple bands antenna and high efficiency rectifier design for RF energy harvesting at 900, 1900 and 2400 MHz," in *IEEE MTT-S Int. Microw. Symp. Dig.*, Seattle, WA, USA, Jun. 2013, pp. 1–3.

[12] D. Masotti, A. Costanzo, M. Del Prete, and V. Rizzoli, "Genetic-based design of a tetra-band high-efficiency radio-frequency energy harvesting system," *IET Microw., Antennas Propag.*, vol. 7, no. 15, pp. 1254–1263, Dec. 2013.

[13] J. Kimionis, M. Isakov, B. S. Koh, A. Georgiadis, and M. M. Tentzeris, "3D-printed origami packaging with inkjet-printed antennas for RF harvesting sensors," *IEEE Trans. Microw. Theory Techn.*, vol. 63, no. 12, pp. 4521–4532, Dec. 2015.

[14] J. Kimionis and M. M. Tentzeris, "RF tag front-end design for uncompromised communication and harvesting," in *Proc. IEEE RFID Technol. Appl. Conf. (RFID-TA)*, Tampere, Finland, Sep. 2014, pp. 109–114.

[15] R. M. Fano, "Theoretical limitations on the broadband matching of arbitrary impedances," Res. Lab. Electron., Massachusetts Inst. Technol., Cambridge, MA, USA, Tech. Rep. 41, Jan. 1948.

[16] F. Bolos, D. Belo, and A. Georgiadis, "A UHF rectifier with one octave bandwidth based on a non-uniform transmission line," in *IEEE MTT-S Int. Microw. Symp. Dig.*, May 2016, pp. 1–3.

[17] H. Oraizi, "Design of impedance transformers by the method of least squares," *IEEE Trans. Microw. Theory Techn.*, vol. 44, no. 3, pp. 389–399, Mar. 1996.

[18] Y.-W. Hsu and E. F. Kuester, "Direct synthesis of passband impedance matching with nonuniform transmission lines," *IEEE Trans. Microw. Theory Techn.*, vol. 58, no. 4, pp. 1012–1021, Apr. 2010.

[19] L. Ranzani, P. Boffi, R. Siano, S. Rondineau, Z. Popovic, and M. Martinelli, "Microwave-domain analog predistortion based on chirped delay lines for dispersion compensation of 10-Gb/s optical communication signals," *J. Lightw. Technol.*, vol. 26, no. 15, pp. 2641–2646, Aug. 1, 2008.

[20] F. Bolos, J. Blanco, A. Collado, and A. Georgiadis, "RF energy harvesting from multi-tone and digitally modulated signals," *IEEE Trans. Microw. Theory Techn.*, vol. 64, no. 6, pp. 1918–1927, Jun. 2016.

[21] J. Bito, J. G. Hester, and M. M. Tentzeris, "Ambient RF energy harvesting from a two-way talk radio for flexible wearable wireless sensor devices utilizing inkjet printing technologies," *IEEE Trans. Microw. Theory Techn.*, vol. 63, no. 12, pp. 4533–4543, Dec. 2015.

[22] J. Kimionis and M. M. Tentzeris, "Pulse shaping: The missing piece of backscatter radio and RFID," *IEEE Trans. Microw. Theory Techn.*, vol. 64, no. 12, pp. 4774–4788, Dec. 2016.

[23] S. Abbasian and T. Johnson, "High efficiency GaN HEMT synchronous rectifier with an octave bandwidth for wireless power applications," in *IEEE MTT-S Int. Microw. Symp. Dig.*, San Francisco, CA, USA, May 2016, pp. 1–4.

John Kimionis (S'10) received the diploma and M.Sc. degrees in electronic and computer engineering from the Technical University of Crete, Chania, Greece, in 2011 and 2013, respectively. He is currently pursuing the Ph.D. degree at the School of Electrical and Computer Engineering, Georgia Institute of Technology, Atlanta, GA, USA.

He was with the Telecom Laboratory, Technical University of Crete. He is currently a Research Assistant with the ATHENA Group, Georgia Institute of Technology. His current research interests include spectral-efficient and energy-efficient backscatter radio and RFID, software-defined radio for sensor networks, RF front-end design for wireless sensors, and additive manufacturing techniques.

Mr. Kimionis was recipient of fellowship awards for his undergraduate and graduate studies. He was a recipient of the First Best Student Paper Award of the IEEE International Conference on RFID-Technologies and Applications (RFID-TA) 2014, Tampere, Finland, as well as the Second Best Student Paper Award of the IEEE International Conference on RFID-Technologies and Applications (RFID-TA) 2011, Sitges, Barcelona, Spain. In 2016, he was a co-recipient of the Bell Labs Award Competition 3rd Prize. He has been a member of the IEEE Microwave Theory and Techniques Society, the IEEE Communications Society, and a Board Member of the IEEE MTT-24 RFID Technologies Committee. He is a Texas Instruments Scholar for his mentoring service for the Opportunity Research Scholars Program of the Georgia Institute of Technology.

Ana Collado (M'08–SM'12) received the M.Sc. and Ph.D. degrees in telecommunications engineering from the University of Cantabria, Santander, Spain, in 2002 and 2007, respectively.

From 2007 to 2016, she was a Senior Research Associate and the Project Management Coordinator with the Technological Telecommunications Center of Catalonia, Barcelona, Spain. Since 2016, she was an Assistant Professor with the Microwaves and Antennas Research Group, School of Engineering and Physical Sciences, Heriot-Watt University, Edinburgh, U.K. She has co-authored over 90 papers in journals and conferences. Her current research interests include active antennas, substrate integrated waveguide structures, nonlinear circuit design, and energy harvesting and wireless power transmission solutions for self-sustainable and energy-efficient systems.

Dr. Collado serves on the Editorial Board of the *Radioengineering Journal* and she is currently an Associate Editor of *IEEE Microwave Magazine*, an Associate Editor of the *IET Microwaves*, *Antennas and Propagation journal*, a member of the Editorial Board of the *Cambridge Wireless Power Transfer Journal*, IEEE MTT-26 Wireless Energy Transfer and Conversion, and MTT-24 RFID Technologies. She has participated in national and international research projects. She has collaborated in the organization of several international workshops in different countries of the European Union and a training school for Ph.D. students.

Manos M. Tentzeris (S'89–M'92–SM'03–F'10) received the diploma degree (*magna cum laude*) in electrical and computer engineering from the National Technical University of Athens, Athens, Greece, and the M.S. and Ph.D. degrees in electrical engineering and computer science from the University of Michigan, Ann Arbor, MI, USA.

He is currently a Ken Byers Professor of flexible electronics with the School of Electrical and Computer Engineering, Georgia Institute of Technology, Atlanta, GA, USA. He served as the Head of the GT-ECE Electromagnetics Technical Interest Group, the Georgia Electronic Design Center Associate Director for RFID/Sensors Research, the Georgia Tech NSF-Packaging Research Center Associate Director for RF Research, and the RF Alliance Leader. He has helped develop academic programs in 3-D/inkjet-printed RF electronics and modules, flexible electronics, origami and morphing electromagnetics, highly integrated/multilayer packaging for RF and wireless applications using ceramic and organic flexible materials, paper-based RFID's and sensors, wireless sensors and biosensors, wearable electronics, "green" electronics, energy harvesting and wireless power transfer, nanotechnology applications in RF, microwave MEM's, SOP-integrated (UWB, multiband, millimeter wave, and conformal) antennas and heads the ATHENA Research Group (20 researchers). He was a Visiting Professor with the Technical University of Munich, Germany for the summer of 2002, a Visiting Professor with GTRI-Ireland in Athlone, Ireland for the summer of 2009 and a Visiting Professor with LAAS-CNRS in Toulouse, France for the summer of 2010. He has given more than 100 invited talks to various universities and companies all over the world. He has authored more than 650 papers in refereed journals and conference proceedings, 5 books, and 25 book chapters.

Dr. Tentzeris was a recipient or co-recipient of the 2017 Georgia Tech Outstanding Achievement in Research Program Development Award, 2016 Bell Labs Award Competition 3rd Prize, the 2015 IET Microwaves, Antennas and Propagation Premium Award, the 2014 Georgia Tech ECE Distinguished Faculty Achievement Award, the 2014 IEEE RFID-TA Best Student Paper Award, the 2013 IET Microwaves, Antennas and Propagation Premium Award, the 2012 FiDiPro Award in Finland, the iCMG Architecture Award of Excellence, the 2010 IEEE Antennas and Propagation Society Piergiorgio L. E. Uslenghi Letters Prize Paper Award, the 2011 International Workshop on Structural Health Monitoring Best Student Paper Award, the 2010 Georgia Tech Senior Faculty Outstanding Undergraduate Research Mentor Award, the 2009 IEEE TRANSACTIONS ON COMPONENTS AND PACKAGING TECHNOLOGIES Best Paper Award, the 2009 E. T. S. Walton Award from the Irish Science Foundation, the 2007 IEEE AP-S Symposium Best Student Paper Award, the 2007 IEEE MTT-S IMS Third Best Student Paper Award, the 2007 ISAP 2007 Poster Presentation Award, the 2006 IEEE MTT-S Outstanding Young Engineer Award, the 2006 Asia–Pacific Microwave Conference Award, the 2004 IEEE TRANSACTIONS ON ADVANCED PACKAGING Commendable Paper Award, the 2003 NASA Godfrey "Art" Anzic Collaborative Distinguished Publication Award, the 2003 IBC International Educator of the Year Award, the 2003 IEEE CPMT Outstanding Young Engineer Award, the 2002 International Conference on Microwave and Millimeter-Wave Technology Best Paper Award (Beijing, China), the 2002 Georgia Tech-ECE Outstanding Junior Faculty Award, the 2001 ACES Conference Best Paper Award, the 2000 NSF CAREER Award, and the 1997 Best Paper Award of the International Hybrid Microelectronics and Packaging Society. He was the TPC Chair of the IEEE IMS 2008 Symposium and the Chair of the 2005 IEEE CEM-TD Workshop, and he is the Vice-Chair of the RF Technical Committee (TC16) of the IEEE CPMT Society. He is the Founder and the Chair of the RFID Technical Committee (TC24) of the IEEE MTT Society and the Secretary/Treasurer of the IEEE C-RFID. He is an Associate Editor of the IEEE TRANSACTIONS ON MICROWAVE THEORY AND TECHNIQUES, the IEEE TRANSACTIONS ON ADVANCED PACKAGING and the *International Journal on Antennas and Propagation*. He is a member of URSI-Commission D, a member of MTT-15 Committee, an Associate Member of EuMA, a Fellow of the Electromagnetic Academy, and a member of the Technical Chamber of Greece. He served as one of the IEEE MTT-S Distinguished Microwave Lecturers from 2010 to 2012 and is one of the IEEE CRFID Distinguished Lecturers.

Apostolos Georgiadis (S'94–M'02–SM'08) was born in Thessaloniki, Greece. He received the B.S. degree in physics and M.S. degree in telecommunications from the Aristotle University of Thessaloniki, Thessaloniki, Greece, in 1993 and 1996, respectively, and the Ph.D. degree in electrical engineering from the University of Massachusetts, Amherst, MA, USA, in 2002.

In 2002, he joined Global Communications Devices, North Andover, MA, USA, as a Systems Engineer where he involved in CMOS transceivers for wireless network applications. In 2003, he joined Bermai Inc., Minnetonka, MN, USA, as an RF/Analog Systems Architect. In 2005, he joined the University of Cantabria, Santander, Spain, as a Juan de la Cierva Fellow Researcher. In 2006, he was a consultant for Bitwave Semiconductor, Lowell, MA, USA. He collaborated with ACORDE S.A., Santander, Spain, where he was involved in the design of integrated CMOS VCOs for ultra-wideband applications. In 2007, he joined the Technological Telecommunications Center of Catalonia (CTTC), Spain, as a Senior Researcher of communications subsystems. From 2013 to 2016, he was a Group Leader with the Microwave Systems and Nanotechnology Department, CTTC. In 2016, he joined Heriot-Watt University, Edinburgh, U.K., as an Associate Professor. He has authored more than 160 papers in peer-reviewed journals and international conferences. His current research interests include energy harvesting and wireless power transmission, RFID technology, active antennas and phased-array antennas, inkjet and 3-D printed electronics, millimeter-wave systems.

Dr. Georgiadis was the recipient of a Fulbright Scholarship for graduate studies at the University of Massachusetts, Amherst, in 1996. He was the General Chair of the 2011 IEEE RFID-TA Conference and a General Co-Chair of the 2011 IEEE MTT-S IMWS on Millimeter Wave Integration Technologies. He is an EU Marie Curie Global Fellow. He is member of the IEEE MTT-S TC-24 RFID Technologies (past Chair) and the member of the IEEE MTT-S TC-26 Wireless Energy Transfer and Conversion. He was an Associate Editor of the *IET Microwaves Antennas and Propagation Journal*, IEEE MICROWAVE AND WIRELESS COMPONENTS LETTERS, and the IEEE RFID VIRTUAL JOURNAL. He serves as an Associate Editor of the IEEE JOURNAL ON RFID and he is the Founder and an Editor-in-Chief of the *Wireless Power Transfer Journal* of Cambridge University Press. He is Vice Chair of URSI Commission D, Electronics and Photonics and AdCom member of the IEEE Council on RFID serving as a Vice President of Conferences. He is a Distinguished Lecturer of the IEEE Council on RFID. In 2016, his proposal for Inkjet/3-D printed millimeter-wave systems received the Bell Labs Prize, 3rd Place among more than 250 proposals recognizing ideas that "change the game" in the field of information and communications technologies.